SLAC-PUB-7077
June 1996

Neutron Sources in the Varian Clinac 2100C/2300C Medical Accelerator Calculated by the EGS4 Code

X. S. Mao, K. R. Kase, J. C. Liu and W. R. Nelson
Stanford Linear Accelerator Center
Stanford University, Stanford, CA 94309, USA

J. H. Kleck and S. Johnsen
Varian Associates, Inc., Palo Alto, CA 94304, USA

Abstract - The photoneutron yields produced in different components of the medical accelerator heads evaluated in these studies (24-MV Clinac 2500 and a Clinac 2100C/2300C running in the 10-MV, 15-MV, 18-MV and 20-MV modes) were calculated by the EGS4 Monte Carlo code using a modified version of the Combinatorial Geometry of MORSE-CG. Actual component dimensions and materials (i.e., targets, collimators, flattening filters, jaws and shielding for specific accelerator heads) were used in the geometric simulations. Calculated relative neutron yields in different components of a 24-MV Clinac 2500 were compared with the published measured data, and were found to agree to within ±30%. Total neutron yields produced in the Clinac 2100/2300, as a function of primary electron energy and field size, are presented. A simplified Clinac 2100/2300C geometry is presented to calculate neutron yields, which were compared with those calculated by using the fully-described geometry.

(Submitted to the Health Physics Society)

* Work supported by the U. S. Department of Energy under contract DE-AC-03-76SF00515

INTRODUCTION

Neutrons can be produced by electron beams through electroproduction and photonuclear reactions. In general, the cross sections of electroproduction are expected to be on the order of the fine structure constant, $\alpha \approx 1/137$, times the cross sections of photonuclear reactions. In medical accelerators, the neutrons produced directly by the electron beam are not important. Photoneutrons produced by the giant dipole resonance (GDR) reaction dominate. GDR neutrons are produced by photons with energies from approximately 6 to 35 MeV. The GDR neutron yields are proportional to the product of the length, l, of the material traversed by photons of each energy (i.e., photon track length) and the GDR photoneutron cross section. The photon track length as a function of photon energy, k, is expressed as the differential photon track length, $\frac{dl}{dk}$, representing the total track length of all photons with energies in the interval $k, k+dk$.

Neutrons coming from medical accelerators may require additional shielding and maze to protect personnel outside accelerator rooms. Neutrons produced in different components of the Varian Clinac 35 head have been estimated by McCall and Swanson (1979) using a simple method. Their geometric model consisted of a target, a primary collimator with a 28° opening, a flattening filter and jaws. The estimation was made by use of an approximate yield method developed by Swanson (1978, 1979).

In the present paper, the fully-described geometry (i.e., actual component dimensions and materials for specific accelerator heads) were used as input data in the geometric simulations. The EGS4 code (Nelson et al., 1985) was used to score the track length of each photon. The GDR neutron yields were calculated by integrating the product of the differential photon track length

and the published GDR photoneutron cross sections (Dietrich and Berman, 1988) over the photon energy (see Fig. 1).

METHODS

Details regarding the method used to calculate GDR photoneutron yields have been described in a recent publication (Mao et al., 1996). To simulate actual medical accelerator heads, the Combinatorial Geometry (CG) package from the MORSE-CG code (Emmett, 1984) was used with the EGS4 code. The following geometric bodies were used in the CG-description of the accelerator heads: right parallelepiped, sphere, right circular cylinder, right cone, right angle wedge, truncated right cone, box and arbitrary polyhedron. A total of 85 geometric bodies were included in the Clinac 2100/2300C simulation (Fig. 2). Input data consisted of beam parameters, geometric bodies, the definition of components, materials in the components, and the identification of photoneutron cross sections associated with each material.

As an aid to clinical applications, the neutron yield (neutron per incident electron) can be related to the photon absorbed dose in a water phantom located at the isocenter (one meter from the target) by determining the relationship between the dose delivered and the electron charge at the target. This relationship has been measured for Clinac 2100C accelerators by observing the target-current pulse using a digital oscilloscope (Tektronix TDs) and determining the integral volt-seconds in the waveform. The charge in the pulse was calculated from the ratio (20 mA/V) produced by the 50 ohm terminating resistor connected to the target. Waveform averaging was used to reduce the uncertainties caused by noise and pulse-to-pulse variations. Pulse repetition rate was also determined using the oscilloscope, enabling the calculation of average target current.

The validity of this technique was demonstrated by comparing target current measurements to direct integrals of the target current that were made with a current integrator (ORTEC 439). The charge per pulse measured with the integrator was within 3% of the value determined using the oscilloscope. This was well within the experimental uncertainties.

Because the values obtained by the procedures described above are related to the *measured* target current and not the current *incident* on the target, the fraction of incident electron charge that is deposited in the various targets must be determined. The relationship between the number of electrons incident on the target and the integrated charge collected at the target was determined from a calculation using the EGS4 code. Table 1 gives the beam and the dose parameters for the Clinac 2100C, including the measured kinetic energy of electron beams hitting the target, the measured charge collected in the target per unit photon dose delivered in the isocenter, and the calculated number of electrons incident on the target per unit charge deposited in the target.

RESULTS AND DISCUSSION

Validation of calculation

To determine the accuracy of our method, an EGS4 model was constructed to compare with measurements by Barber and George (1959) for 34 MeV electrons striking targets of aluminum, copper, tantalum, and lead (each approximately one-radiation length thick). Table 2 shows that the calculated yields are systematically lower than the measured yields, but agree to within 30%. Uncertainties in the cross sections (±20%) and the measurement error (±15%) probably account for the differences, since the accuracy of the EGS4

code is better than 5% and the statistical uncertainties in these calculations is of the order of ±1%.

To validate the geometric simulation, further comparisons were made between relative neutron yields calculated by the EGS4 code and the measured relative yields in a 24-MV Clinac 2500 (LaRiviere 1985). LaRiviere's measurement was based on the assumption that the thermal neutron fluence in a cavity (e.g., a room) with concrete walls is uniform inside the cavity and is proportional to the fast neutron source strength. This assumption, in turn, is based on well-established measurements made by Patterson and Wallace (1958) for point istotropic, fast-neutron sources inside concrete enclosures. Bare indium foils distributed in the concrete room were used to measure thermal neutrons. Exposures were made of various stages during the Clinac 2500 assembly, as different components were added. The cumulative gamma counts (corrected for time) from indium foils represented the cumulative neutron source strength of the machine. The neutron yield produced by a major subassembly was proportional to the difference in counts from the indium foils before and after that subassembly was installed. The relative neutron yield in a subassembly was equal to the ratio of the indium-foil counts associated with this subassembly to the total cumulative counts when all components are assembled. The measured relative neutron source strengths shown in Table 3 were significant to about ±10%. It should be noted that the neutron yield associated with a component (for example, a target) in Table 3 was not limited to only those neutrons produced inside the target, but also included neutrons produced in other components (for example, supports and shielding) that were assembled before the target was added. The calculated relative neutron yields agree with the measured data within ±30%, except for neutrons produced in jaws with a field of 40 cm × 40 cm opening.

In this case, the higher neutron yield in the measurement can be attributed to components associated with the jaws, such as supports and shielding, which were not included in the calculation.

Fully-described geometry for Varian Clinac 2100C/2300C

The Varian Clinac 2100/2300C can run in a variety of energy modes and the geometry of the head is quite complicated (Fig. 2). The calculated neutron yields produced in different components (with jaws closed i.e. file size is zero) are listed in Table 4. The materials, from which the components were made, are also shown in the table. The majority of the neutrons were produced in components made of tungsten having a GDR photoneutron threshold of 6.2 MeV, which is much smaller than the 9.91 MeV threshold for copper (Dietrich and Berman, 1988). The yield cross section for tungsten is also significantly larger than copper, as illustrated in Fig. 1.

As expected, the total neutron yield decreases as the electron energies become smaller. This is explained in Fig. 1, which shows that the differential photon track length decreases dramatically in the energy range of the photoneutron reactions as the electron energy is reduced from 20 to 10 MeV. The relative yield of neutrons for each of these modes (with jaws closed) is 1 : 0.55 : 0.21 : 0.006 for 20-MV (22.3 MeV), 18-MV (18.8 MeV), 15-MV (14.9 MeV) and 10-MV (10.3 MeV), respectively.

The total neutron yield produced in accelerator heads is inversely proportional to the field size, as shown in Fig. 3. In the calculations, it was found that neutron yields in components other than the jaws do not change as the field size changes. Furthermore, scattered photons from the jaws are lower in energy and are less likely to produce neutrons. Hence, the decrement of total neutron yield in the head, as the jaws open, is almost the same as the decrement of the neutron yield produced in the jaws. As the field

size increases the jaws retract and, because they are shielded by the primary collimator, they are exposed to fewer photons. The photon spatial energy-fluence distribution around the jaws is relatively uniform when the field size is less than 20 cm. As a result, the neutron yield produced in the jaws, and therefore the total neutron yield in the head, decreases linearly as the field size increases (Fig. 3).

Simplified geometry for Varian Clinac 2100/2300C

The fully-described geometry represented all the major components in a Clinac 2100/2300C in above discussion. A simplified geometry was also created, in which the target, primary collimator, flattening filter, and jaws were almost the same as the fully-described geometry, but other components (e.g., magnets, secondary collimator and shielding, etc.) were simulated by several spheres as illustrated in Fig. 4. Only 22 geometric bodies were used and the neutron yields for this simplified geometry are listed in Table 5. The total neutron yields in Table 5 agree with those in Table 4 very well. Calculated neutron yields for the major components in Table 5 agree with those in Table 4 within ±6%. Both the simplified model and the fully-described model will be used in future studies involving transport of the neutrons themselves in accelerator heads.

CONCLUSIONS

By means of the EGS4 code, together with the MORSE-CG Combinatorial Geometry scheme for modeling the actual accelerator heads, estimates have been made of the neutron yields in various head components of a 24-MV Clinac 2500, with agreement to better than ±30% compared to previous measurements. The accelerator head of a 20-MV Clinac 2100/2300C (with jaws closed) was also simulated and a total neutron yield of 2.2×10^{-3} neutron

per incident electron was obtained. The total neutron yield produced in the head of a Clinac 2100/2300C decreases dramatically when the electron energy is reduced to 10 MeV. The relative total neutron yield (with jaws closed) was found to be 1 : 0.55 : 0.21 : 0.006 for operation of a Clinac 2100/2300C running at the 20, 18, 15 and 10-MV energy modes, respectively. It was also observed that the total neutron yield produced in these accelerator heads decreased linearly as the jaws were opened.

This work is the beginning of a series of radiation studies on the Varian Clinac 2100/2300C. Results of calculations of the neutron fluence and spectra at various locations outside the accelerator head will be published separately.

Acknowledgments -- The authors express their sincere appreciation of Dr. R. C. McCall and P. D. LaRiviere, whose discussion on the neutron-yield calculation and measurement was very helpful. We also thank Dr. Keith Wise of the Australian Radiation Laboratory for reading the manuscript and for general support during his stay in our laboraory.

REFERENCES

Barber, W. C.; George W. D. Neutron yields from targets bombarded by electrons. Phys. Rev. 116: 1551-1559; 1959.

Emmett, M. B. The MORSE Monte Carlo radiation transport code system. ORNL-4972 , Oak Ridge National Laboratory; 1984.

LaRiviere, P. D. Neutron sources in a 24-MV medical linear accelerator. Med. Phys. 12: 806-809; 1985.

Mao, X.; Kase, K. R.; Nelson, W. R. Giant dipole resonance neutron yields produced by electrons as a function of target material and thickness. Health Physics. 70: 1-7; 1996.

McCall, R. C.; Swanson, W.P. Neutron sources and their characterictic. NBS-554, National Bureau of Standards; 1979.

Nelson, W. R.; Hirayama, H.; Rogers, D. W. O. The EGS4 code system. SLAC-265, Stanford Linear Accelerator Center; 1985.

Patterson, H. W,; Wallace, R. W.; A method of calibrating slow-neutron detectors. UCRL-8359, Lawrence Berkeley Laboratory; 1958.

Swanson, W. P. Calculation on neutron yields released by electrons incident on selected materials. Health Physics 35: 353-367; 1978.
Swanson, W. P. Improved calculation of photoneutron yields released by incident electrons. Health Physics 37: 347-358; 1979.

Captions for figures

Fig. 1. a) Total photoneutron yield cross sections for tungsten and copper; b) Differential photon track length distributions produced in 1-radiation length-thick tungsten targets struck by 10 MeV, 15 MeV, and 20 MeV electrons.

Fig. 2. Fully-described geometry for the Varian Clinac 2100/2300C. The slice is at y=0, showing the electron-beam trajectory entering from the left along the accelerator waveguide, passing through a bending magnet and into the target.

Fig. 3. Total neutron yield produced in Clinac 2100/2300C as a function of field size for various electron energies (normalized to zero field size, i.e., jaws closed).

Fig. 4. Simplified Combinatorial Geometry for a Clinac 2100/2300C.

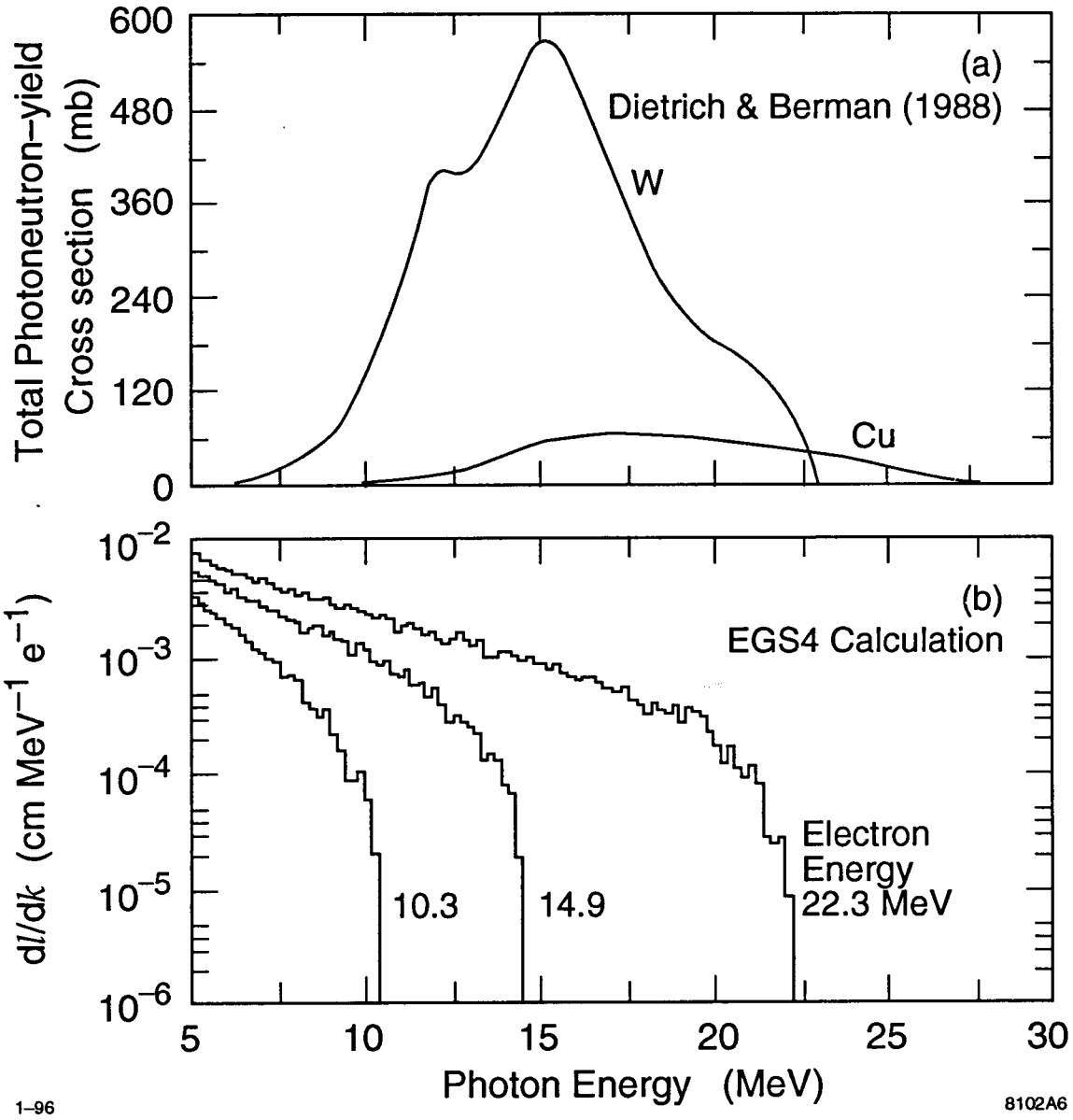
Total Photoneutron–yield
Cross section (mb)
600
480
360
240
120
0
(a)
Dietrich & Berman (1988)
W
Cu
dI/dk (cm MeV^{-1} e^{-1})
10^{-2}
10^{-3}
10^{-4}
10^{-5}
10^{-6}
(b)
EGS4 Calculation
Electron
Energy
22.3 MeV
14.9
10.3
5
10
15
20
25
30
Photon Energy (MeV)
1–96
8102A6

Fig. 1

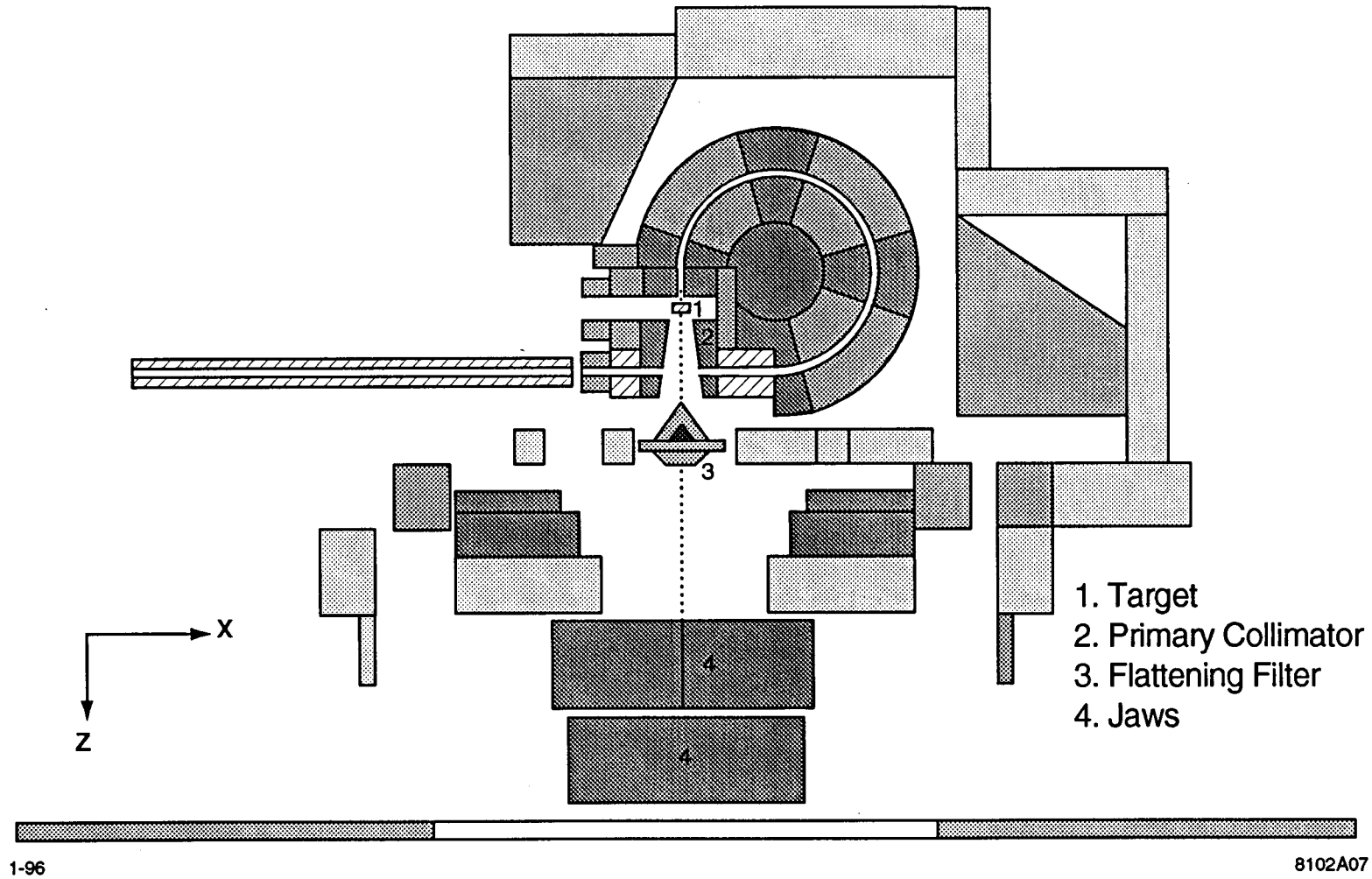
1
2
3
4
4
X
Z
1. Target
2. Primary Collimator
3. Flattening Filter
4. Jaws
1-96
8102A07

Fig. 2

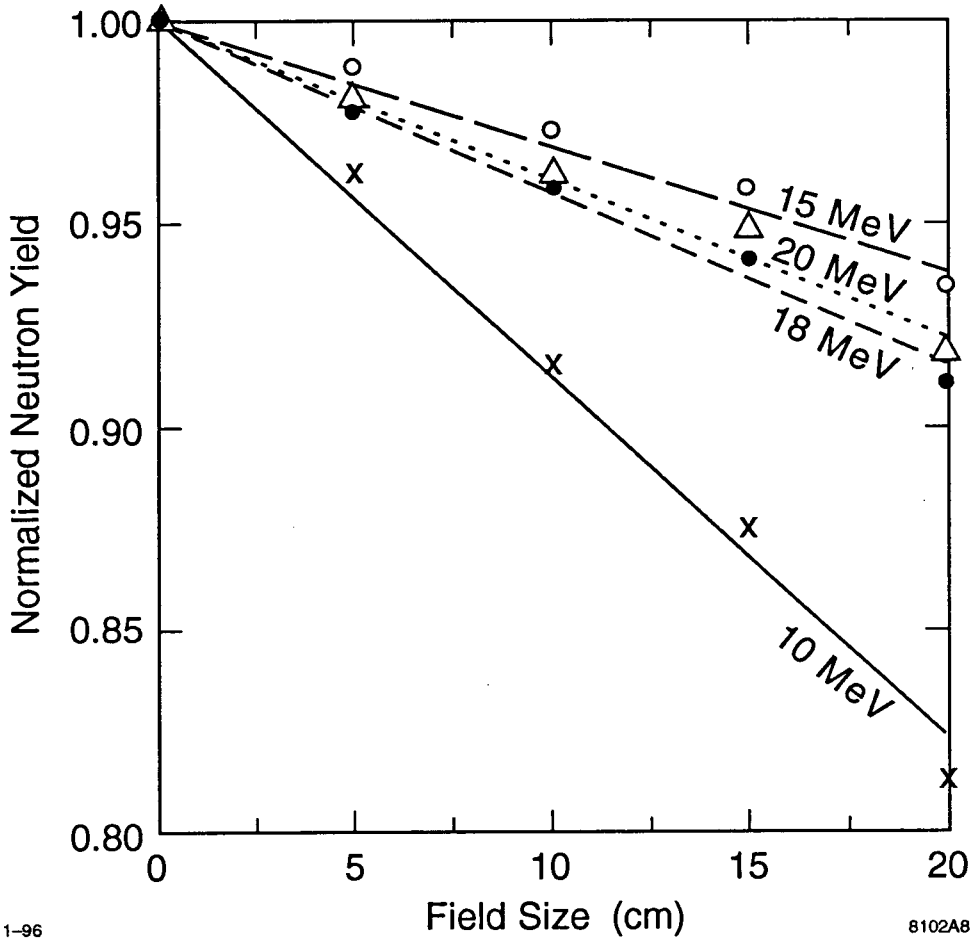
1.00
0.95
0.90
0.85
0.80
Normalized Neutron Yield
0
5
10
15
20
Field Size (cm)
15 MeV
20 MeV
18 MeV
10 MeV
1–96
8102A8

Fig. 3

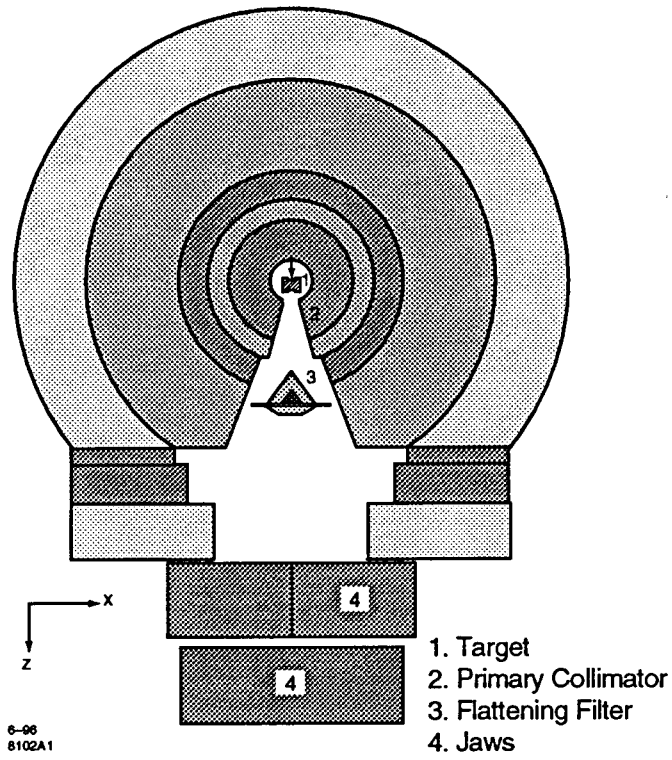
1
2
3
4
4
X
Z
6-96
8102A1
1. Target
2. Primary Collimator
3. Flattening Filter
4. Jaws

Fig. 4

Table 1. The beam and the dose parameters for Clinac 2100C*

Mode	Kinetic energy of electron beam hitting target (Measurement) MeV	Charge collected by target per photon dose in isocenter (Measurement) $\mu C\ Gy^{-1}$	Incident Charge per charge deposited in target (EGS4 calculation) %	Incident electrons per charge deposited in target (EGS4 calculation) μC^{-1}	Incident electrons per photon dose in isocenter Gy^{-1}
20 MV	22.3	81	1.108	6.92×10^{12}	5.6×10^{14}
18 MV	18.8	160	1.058	6.61×10^{12}	1.0×10^{15}
15 MV	14.9	230	1.050	6.55×10^{12}	1.5×10^{15}
10 MV	10.3	440	1.066	6.66×10^{12}	2.9×10^{15}

* The Clinac 2100C data apply also to the Clinac 2300C.

Table 2. Neutron yields produced by 34 MeV electron beams (normalized to incident electron)

Target material	Target thickness		Measured neutron yield[a]	Neutron yield Calculated by EGS4	measured/calculated
	radiation length	cm	(10^{-5} MeV^{-1})	(10^{-5} MeV^{-1})	
Aluminum	1.00	8.9	1.3 ± 0.2	0.98	1.3
Copper	1.04	1.49	3.8 ± 0.6	3.0	1.3
Tantalum	0.98	0.40	5.3 ± 0.8	5.0	1.1
Lead	1.01	0.57	6.2 ± 0.9	4.9	1.3

[a] Measured data are from Barber and George (1959).

Table 3. Neutron sources in Varian 24-MV Clinac 2500

Component	Measured relative neutron yield[a] %	Relative neutron yield Calculated by EGS4	measured/calculated	Measured relative neutron yield[a] %	Relative neutron yield Calculated by EGS4	measured/calculated
Field size (cm^2)	0 x 0 0	0 x 0 0		40 x 40 1600	40 x 40 1600	
Target (W, Cu)	28	23	1.3	33	27	1.2
Primary collimator (W)	35	45	0.8	42	53	0.8
Flattening filter (Fe)	9	10	0.9	11	12	0.9
Secondary collimator (Pb) and Jaws (W)	28	23	1.2	14	8	1.8

[a] Measured data are from LaRiviere (1985).

Table 4. Calculated Neutron sources in Varian Clinac 2100/2300 (Actual geometry with Jaws closed)

	Mode 20 MV energy on target 22.3 MeV		Mode 18 MV energy on target 18.8 MeV		Mode 15 MV energy on target 14.9 MeV		Mode 10 MV energy on target 10.3 MeV	
Component	Neutron yield per incident electron	Relative neutron yield %	Neutron yield per incident electron	Relative neutron yield %	Neutron yield per incident electron	Relative neutron yield %	Neutron yield per incident electron	Relative neutron yield %
Target	3.8×10^{-4} (W, Cu)	17.1	1.9×10^{-4} (W, Cu)	15.5	4.1×10^{-5} (W, Cu)	9.2	1.7×10^{-9} (Cu)	0.013
Primary collimator	7.9×10^{-4} (W)	35.5	4.9×10^{-4} (W)	39.9	1.7×10^{-4} (W)	38.0	5.9×10^{-6} (W)	44.2
Flattening filter	2.3×10^{-4} (Fe, Ta)	10.3	1.1×10^{-4} (Fe, Ta)	9.0	1.0×10^{-4} (W)	22.4	4.5×10^{-9} (Cu)	0.034
Jaws	8.0×10^{-4} (W)	36.0	4.2×10^{-4} (W)	34.2	1.3×10^{-4} (W)	29.1	7.3×10^{-6} (W)	54.7
Others (magnets, shielding, etc.)	2.4×10^{-5}	1.1	1.7×10^{-5}	1.4	5.8×10^{-6}	1.3	1.4×10^{-7}	1.0
Total	2.2×10^{-3}	100.0	1.2×10^{-3}	100.0	4.5×10^{-4}	100.0	1.3×10^{-5}	100.0
Neutron per Gy in isocenter	1.2×10^{12}		1.2×10^{12}		6.8×10^{11}		3.8×10^{10}	

Table 5. Calculated Neutron sources in Varian Clinac 2100/2300 (Simplified geometry with Jaws closed)

	Mode 20 energy on target	MV 22.3 MeV	Mode 18 energy on target	MV 18.8 MeV	Mode 15 energy ontarget	MV 14.9 MeV	Mode 10 energy on target	MV 10.3 MeV
Source	Neutron yield per incident electron	Relative neutron yield %	Neutron yield per incident electron	Relative neutron yield %	Neutron yield per incident electron	Relative neutron yield %	Neutron yield per incident electron	Relative neutron yield %
Target	3.8×10^{-4} (W, Cu)	17.2	1.9×10^{-4} (W, Cu)	15.6	4.1×10^{-5} (W, Cu)	9.0	1.8×10^{-9} (Cu)	0.013
Primary collimator	7.6×10^{-4} (W)	34.5	4.7×10^{-4} (W)	38.4	1.7×10^{-4} (W)	37.5	5.6×10^{-6} (W)	42.7
Flattening filter	2.3×10^{-4} (Fe, Ta)	10.3	1.1×10^{-4} (Fe, Ta)	9.0	1.0×10^{-4} (W)	22.2	4.8×10^{-9} (Cu)	0.035
Jaws	8.2×10^{-4} (W)	37.4	4.4×10^{-4} (W)	36.3	1.4×10^{-4} (W)	30.6	7.4×10^{-6} (W)	56.4
Others (magnets, shielding, etc.)	1.4×10^{-5}	0.64	8.3×10^{-6}	0.68	3.1×10^{-6}	0.68	1.1×10^{-7}	0.87
Total	2.2×10^{-3}	100.0	1.2×10^{-3}	100.0	4.5×10^{-4}	100.0	1.3×10^{-5}	100.0
Neutron per Gy in isocenter	1.2×10^{12}		1.2×10^{12}		6.8×10^{11}		3.8×10^{10}	